THE JOURNAL OF BIOLOGICAL CHEMISTRY VOL. 285, NO. 15, pp. 11219–11226, April 9, 2010

The Microtubule-associated Histone Deacetylase 6 (HDAC6) Regulates Epidermal Growth Factor Receptor (EGFR) Endocytic Trafficking and Degradation*

Received for publication, July 8, 2009, and in revised form, January 4, 2010 Published, JBC Papers in Press, February 4, 2010, DOI 10.1074/jbc.M109.042754

Ya-sheng Gao, Charlotte C. Hubbert, and Tso-Pang Yao[1]

From the Department of Pharmacology and Cancer Biology, Duke University, Durham, North Carolina 27710

Histone deacetylase 6 (HDAC6) is a microtubule-associated deacetylase with tubulin deacetylase activity, and it binds dynein motors. Recent studies revealed that microtubule acetylation affects the affinity and processivity of microtubule motors. These unique properties implicate a role for HDAC6 in intracellular organelle transport. Here, we show that HDAC6 associates with the endosomal compartments and controls epidermal growth factor receptor (EGFR) trafficking and degradation. We found that loss of HDAC6 promoted EGFR degradation. Mechanistically, HDAC6 deficiency did not cause aberrant EGFR internalization and recycling. Rather, it resulted in accelerated segregation of EGFR from early endosomes and premature delivery of EGFR to the late endosomal and lysosomal compartments. The deregulated EGFR endocytic trafficking was accompanied by an increase in microtubule-dependent movement of EGFR-bearing vesicles, revealing a novel regulation of EGFR vesicular trafficking and degradation by the microtubule deacetylase HDAC6.

Endocytosis and subsequent delivery of endosomal cargos to lysosomes are essential for the degradation of many membrane-associated proteins that are critical for cell signaling. This process is crucial for determination of the amplitude of growth factor signaling and is therefore tightly regulated. In this aspect, the complete itinerary starting from the cell surface to the degradative lysosomes near the cell center has been illustrated using the epidermal growth factor (EGF)[2]-activated EGFR as a model system. Activated EGF receptors are first internalized through clathrin-dependent endocytosis. The receptors are then either sorted into the recycling endosomes and return to the cytoplasmic membrane, or are centripetally transported from the early endosomes to the multivesicular bodies (MVBs)/late endosomes before they are dumped into lysosomes for degradation. The lysosomal degradation of EGFR has been identified as a key mechanism to attenuate the EGF signaling. Deregulation of this pathway has been linked to the development and progression of varied types of human cancers (reviewed in Ref. 1). Despite the fact that much effort has been invested in the research of EGFR endocytosis and its intracellular transport, the transition of EGFR from early to late endosomes is still not well understood. Earlier lines of evidence suggest that sorting and transport of early endocytic cargos to later stage endocytic compartments require microtubules and microtubule-associated motors (2–6). However, how microtubules and post-translational modifications on tubulin, especially tubulin acetylation (7), regulate EGFR intracellular trafficking has not been completely elucidated.

Unlike other histone deacetylases with chromatin remodeling activity, HDAC6 catalyzes deacetylation of cytoplasmic substrates, such as α-tubulin, Hsp90, and cortactin (8–11). In HDAC6-deficient cells, the entire microtubule network becomes hyperacetylated (8, 12). Unexpectedly, α-tubulin acetylation alone does not affect microtubule-dependent mitosis or cell migration (12). Instead, recent evidence indicates that α-tubulin acetylation promotes the association of microtubules with dynein and kinesin motors, leading to increased motor processivity and secretory vesicle flux in neurons (13, 14). Together, these results point to a potentially regulatory role for HDAC6 in endocytic cargo transport. While we have previously shown that HDAC6 affects the transport of ubiquitinated misfolded proteins (15), whether HDAC6 regulates the endocytic cargo transport in the vesicular network is still not known. In this report we present evidence that HDAC6 associates with the endosomal compartments and regulates EGFR endocytic trafficking and degradation through modulation of tubulin acetylation.

EXPERIMENTAL PROCEDURES

Cell Lines, Constructs, and siRNA—Human cells lines A549 (lung cancer), 293T (embryonic kidney), LNCaP (prostate cancer), and Panc-1 (pancreatic cancer) were from ATCC and maintained in DMEM (with high glucose, Invitrogen), 10% fetal bovine serum (Invitrogen), penicillin (100 units/ml), and streptomycin (100 μg/ml) (Invitrogen) at 37 °C with 5% CO_2. Stable HDAC6 knock-down A549 cells and their paired control cells have been reported before (15). HDAC6-null mouse embryonic fibroblasts (MEFs) that stably express GFP-tagged HDAC6 constructs were also reported earlier (12). Those MEFs were engineered to stably express EGF receptor through a retrovirus-mediated gene transfer approach using pBABE-hygro plas-

* This work was supported in part, by National Institutes of Health Grant NS053825. This work was also supported by Department of Defense Grants PC 050119 (to Y.-s. G.) and DAMD 17-01-1-0054 and the Leukemia and Lymphoma Society (to T.-P. Y.).

[1] To whom correspondence should be addressed: C325 LSRC, Box 3813, Dept. of Pharmacology and Cancer Biology, Duke University, Research Drive, Durham, NC 27710. Tel.: 919-613-8654; Fax: 919-668-3954; E-mail: yao00001@mc.duke.edu.

[2] The abbreviations used are: EGF, epidermal growth factor; EGFR, EGF receptor; DMEM, Dulbecco's modified Eagle's medium; PBS, phosphate-buffered saline; GFP, green fluorescent protein; WT, wild type; HDAC6, histone deacetylase 6; EEA1, early endosome antigen 1; MEF, mouse embryonic fibroblast; TSA, trichostatin A; MVB, multivesicular body.

mid containing full-length human EGFR sequence. MEFs were maintained and propagated in DMEM (Invitrogen), 10% fetal calf serum (Invitrogen) and penicillin (100 units/ml)/streptomycin (100 μg/ml) at 37 °C with 5% CO_2. pIRESneo-EGFP-α tubulin 1β (16) was purchased from Addgene and the EGFP-α-tubulin 1β fragment was subcloned into pcDNA3.1(+) (Invitrogen) vector between Nhe1 and BamH1 sites (EGFP-α-tubulin WT). α-tubulin point mutations at lysine 40 to arginine (EGFP-α-tubulin K40R) and to glutamine (EGFP-α-tubulin K40Q) were generated by PCR (QuikChange kit, Stratagene). The sequences of all constructs were verified by sequencing. siRNA oligomer targeting HDAC6 (5′-GCUGCACCGUGAGAGUUCCAACUUU-3′) for transient gene silencing was made by Invitrogen.

Antibodies and Reagents—The following antibodies and reagents were used in this study: anti-human HDAC6 (H-300), anti-EGFR (mAb R-1, pAb 1005), anti-phospho-Erk1/2, and anti-Erk1/2 (all from Santa Cruz Biotechnology Inc.); anti-acetyl-α-tubulin (from Dr. M. Yoshida, RIKEN); anti-β-actin (AC-15), Protease Inhibitor Cocktail, Phosphatase Inhibitor Cocktail, Extravdin-HRP, trichostatin A (TSA), cycloheximide, Accutase, and saponin (all from Sigma-Adrich); rabbit anti-GAPDH (Cell Signaling); epidermal growth factor and anti-phosphotyrosine antibody (4G10) (Upstate Cell Signaling Solutions); anti-EEA1 (BD Bioscience); anti-transferrin receptor (Zymed Laboratories Inc.); anti-LAMP2 and anti-CD63 (Developmental Studies Hybridoma Bank); wortmannin (Chemicon); EZ-link Sulfo-NHS-SS-biotin (Pierce); EGF-Alexa Fluor 488 and phalloidin-Alexa Fluor 647 (Invitrogen); goat anti-rabbit IgG rhodamine red X, goat anti-mouse IgG rhodamine red X, goat anti-rabbit IgG Cy5, and goat anti-mouse IgG Cy5 (Jackson ImmunoResearch Laboratories); SuperSignal West Pico Chemiluminescent kit (Pierce Biotechnology). Transfection reagents Lipofactamine siRNA Max, Lipofactamine LTX with PLUS and FuGENE 6 were from Invitrogen and Roche separately. The manufacturers' protocols were followed. Other chemicals were either from Sigma-Aldrich or from Fisher Scientific.

Immunofluorescence Microscopy—Immunostaining was performed as described previously (12). Cells were imaged on a Leica SP5 confocal microscope with ×40 oil objective. 488, 561, and 633 laser lines were used for sequential excitation. Final images were acquired with line-averaging of 4. Brightness and contrast of the images were adjusted in Photoshop CS (Adobe Systems Inc.). For saponin treatment, cells were first rinsed with cold PBS three times and incubated with 0.005% (w/v) saponin that was made freshly in 4 °C PBS. Saponin treatment lasted 5 min on ice and was stopped by quickly rinsing the cells three times with cold PBS. Then regular immunofluorescent microscopy procedure was applied. For EGF treatment, cells were serum-starved in serum-free medium overnight and EGF (100 ng/ml) or EGF-Alexa Fluor 488 (80 ng/ml) made in 37 °C pre-warmed serum-free medium was then added to cells. EGF treatement lasted for 10 min (or indicated times). For wortmannin treatment, serum-starved cells were first pretreated with wortmannin (100 nM in DMSO) for 30 min and then stimulated with EGF in the presence of fresh wortmannin for another 30 min. To evaluate the colocalization between EGFR puncta and those of EEA1 or LAMP2, immunofluorescent images from random fields were analyzed using ImageJ (NIH). For EGFR-EEA1 colocalization, at least 45 cells from 10 random fields at each time point were analyzed; for EGFR-LAMP2 colocalization, at least 30 cells from 5–8 random fields of each time point were analyzed.

Live Cell Imaging—Cells grown on glass coverslips were serum-starved overnight and treated with 80 ng/ml EGF-Alexa Fluor 488. The coverslip was then mounted on a sealed silicon rubber chamber filled with 37 °C pre-warmed medium and 10 mM HEPES as described previously (17). Cells were examined at 37 °C with a ×100 objective on a Zeiss Axio Observer Z1 inverted microscope, which was equipped with stage incubator and outer environmental chamber. Time-lapse imaging started 5 min after EGF treatment with an interval of 1 s for at least 10 min. A Coolsnap ES2 CCD camera (Photometrics) was used for image acquisition, and it was controlled by MetaMorph (Molecular Devices). Time-lapse image stacks were analyzed in MetaMorph that random EGF-Alexa Fluor 488-containing vesicles (they should stay in the same focal plane for at least 10 s) were tracked manually for 10 frames at time points when the cells were treated with EGF-Alexa Fluor 488 for 6, 7, 8, and 9 min. At least 12,000 movement steps from 12 video clips in each cell group were analyzed. The interval velocity of each step was recorded and pooled.

Equilibrium Density Centrifugation—Subcellular fractionation was conducted following a previous protocol (18). Briefly, cell homogenate was prepared in HKM (25 mM Hepes, pH 7.4, 115 mM potassium acetate, 2.5 mM magnesium chloride, and protease inhibitor mixture) and 0.25 M sucrose from 80% confluent A549 cells by passing the cells through 26G5/8 needle 20 times on ice. The post-nuclear supernatant (PNS) was made from cell homogenate by centrifugation at 1,500 × *g* for 10 min. The PNS was mixed with 2 M sucrose (made in HKM) to bring sucrose to 1.6 M. This mixture was loaded at the bottom of the centrifugation tube and was overlaid consecutively with 1.4, 1.2, 1.0, 0.7, and 0.5 M sucrose. Equilibrium centrifugation was carried out in a SW 40Ti swing-bucket rotor (Beckman-Coulter) at 130,000 × g_{max} for 14 h. Fractions were collected from the top and analyzed by a regular immunoblotting procedure.

Endocytosis of EGF Receptor—Cells were serum-starved overnight at 37 °C and then stimulated with EGF (100 ng/ml) for 0, 3, and 10 min separately. The cells were immediately washed with ice-cold PBS and incubated at 4 °C for 45 min with pre-chilled EZ Link-sulfo-NHS-S-S-biotin made in 0.05 M borate buffer (pH 8.0) and 0.15 M NaCl. Then the cells were washed with 0.05 M Tris-buffer saline (TBS) for 2 times (5 min each) and lysed in lysis buffer (TBS, 1% Triton X-100, 1 mM sodium pervanadate, 1 mM phenylmethylsulfonyl fluoride, Protease Inhibitor Cocktail, and Phosphatase Inhibitor Cocktail). Biotinylated membrane proteins were then pulled-down on avidin beads and analyzed by regular immunoblotting procedure using antibodies for EGFR and transferrin receptor.

Biotin-EGF Recycling—A procedure modified from (19) was followed for this assay. Briefly, serum-starved A549 cells were first incubated with 40 ng/ml biotin-EGF (made in DMEM-0.1% bovine serum albumin) for 1.5 h on ice and the non-bound biotin-EGF was washed out once with cold DMEM. Then the

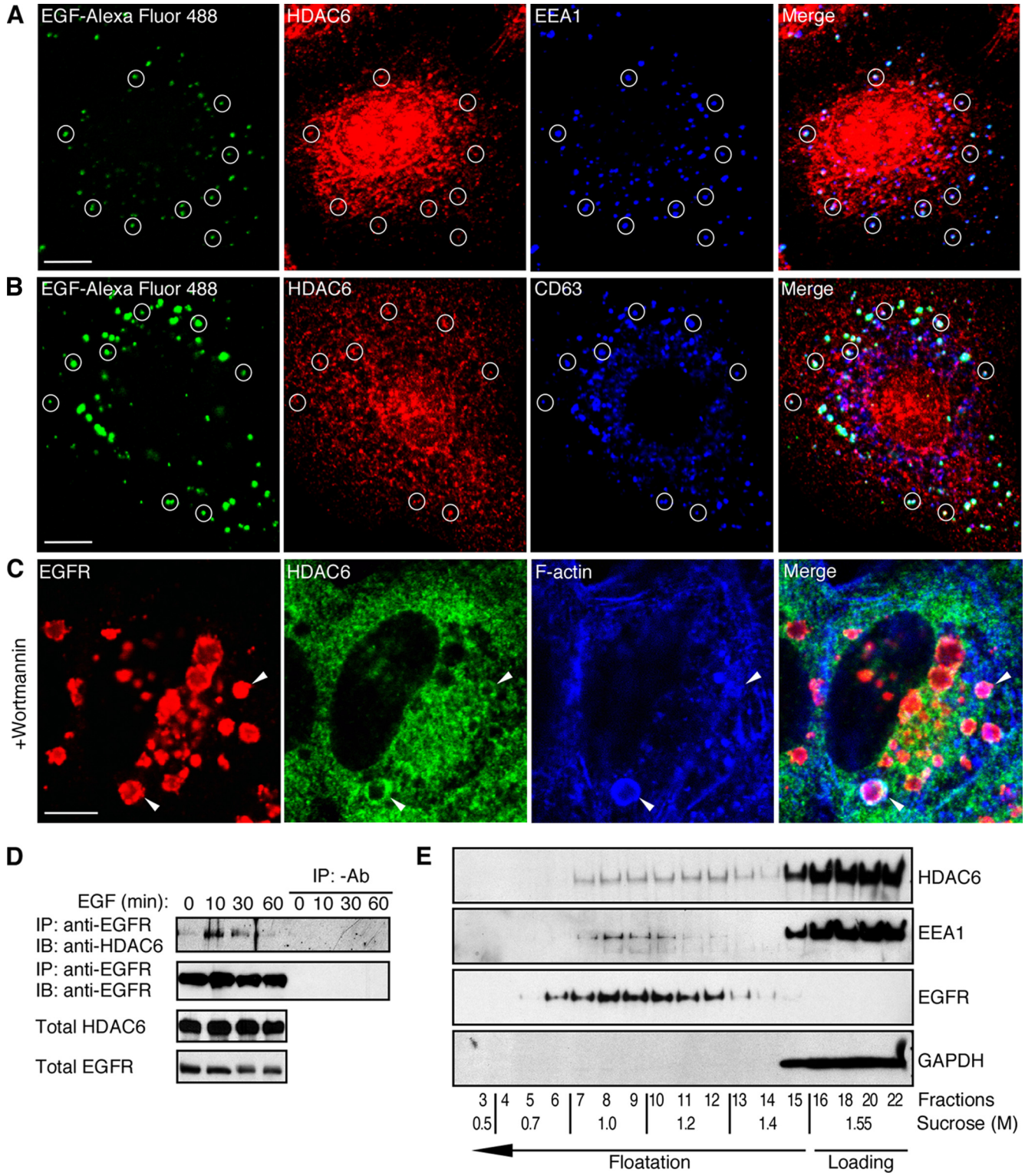

FIGURE 1. **HDAC6 associates with the endosomal compartments.** *A*, A549 cells were serum-starved overnight and treated with 80 ng/ml EGF-Alexa Fluor 488 for 10 min. Cells were then treated with 0.005% saponin before being processed for immunofluorescent microscopy using anti-EEA1 and HDAC6 antibodies. Cycles indicate examples of endosomes that display colocalization of EGF-Alexa Fluor 488 (*green*), EEA1 (*blue*), and HDAC6 (*red*). *Scale bars* throughout this figure: 10 μm. *B*, A549 cells were treated with EGF-Alexa Fluor 488 for 60 min and processed for immunostaining as in *A* using anti-CD63 and HDAC6 antibodies. Representative endosomes that show colocalization of EGF (*green*), CD63 (*blue*), and HDAC6 (*green*) were cycled. *C*, serum-starved A549 cells were pretreated with 100 nM wortmannin and were stimulated with EGF for 30 min. Triple-labeling immunofluorescent microscopy revealed association (*arrowheads*) between EGFR (*red*), HDAC6 (*green*), and F-actin (labeled with Phalloidin-Alexa Fluor 647, *blue*) at the enlarged late endosomes/MVBs. *D*, A549 cells were treated with EGF for indicated times and were processed for immunoprecipitation with monoclonal anti-EGFR antibody or without anti-EGFR antibody. Immunoblotting of the precipitates was carried out using anti-HDAC6 antibody or polyclonal anti-EGFR antibody. Total cell lysates were also examined for HDAC6 and EGFR. *E*, cell homogenate from A549 cells was loaded at the bottom of a discontinuous sucrose gradient and separated by equilibrium density centrifugation. Fractions from top of the tube were collected and analyzed by immunoblotting using anti-HDAC6, anti-EEA1, anti-EGFR, and anti-GAPDH antibodies. A portion of HDAC6 was up-floated in the gradient.

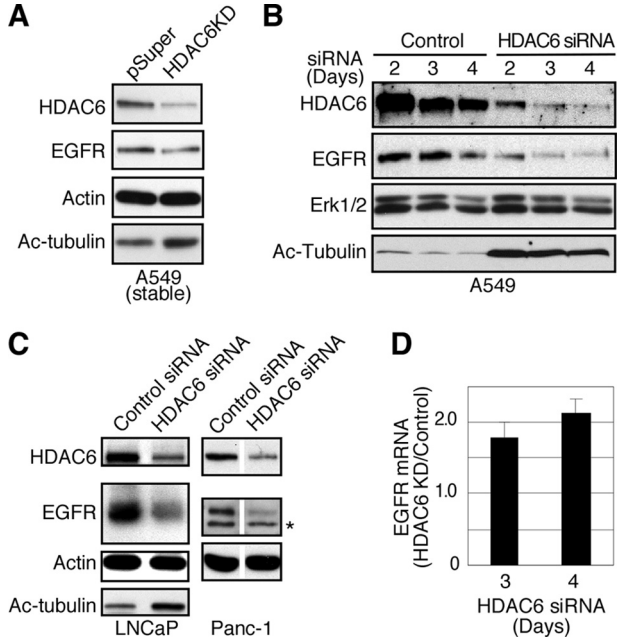

FIGURE 2. **HDAC6 knock-down reduces EGFR stability.** *A*, A549 cells with stable HDAC6 knock-down were examined by immunoblotting for EGFR, HDAC6, acetyl-tubulin, and β-actin. *B*, A549 cells were transfected with control siRNA or HDAC6-targeting siRNA for 2, 3, or 4 days. Cell lysates from both control and HDAC6 siRNA-treated cells were prepared and analyzed by immunoblotting using anti-HDAC6, anti-EGFR, anti-Erk1/2, and anti-acetyl α-tubulin antibodies. EGFR level was reduced in HDAC6 knock-down cells. *C*, LNCaP and Panc-1 cells were transfected with control siRNA or HDAC6-targeting siRNA for 3 days. Cell lysates from both control and HDAC6 knock-down cells were analyzed by immunoblotting using anti-HDAC6, anti-EGFR, anti-β-actin, and anti-acetyl α-tubulin antibodies. *, unidentified band. *D*, HDAC6 was transiently knocked down for 3 or 4 days as in *B*. EGFR transcripts were prepared and amplified by real-time PCR. EGFR mRNA from HDAC6 knock-down cells was compared with that from control cells. Average values from triplicate wells are shown.

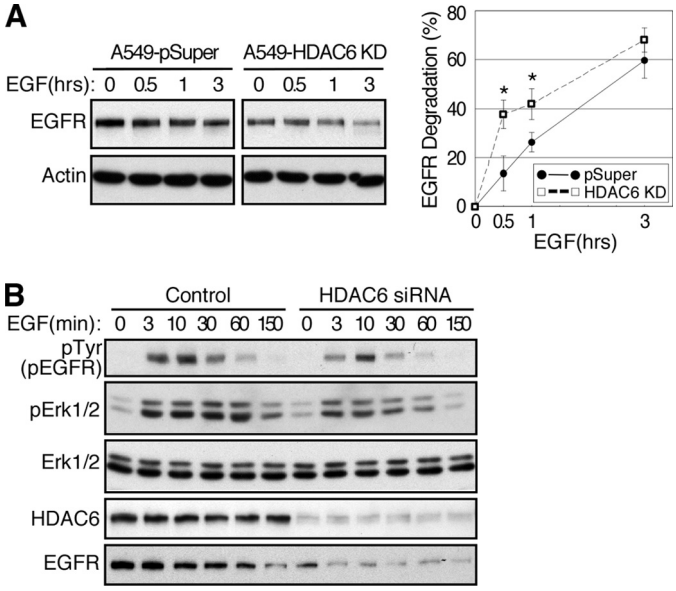

FIGURE 3. **EGFR degradation is promoted in HDAC6-deficient cells.** *A*, control and stable HDAC6 knock-down A549 cells were serum-starved and stimulated with 100 ng/ml EGF in the presence of 10 μg/ml cycloheximide for indicated times. Cell lysates were examined for EGFR and β-actin by immunoblotting. A representative result was shown in the *left panel*. In the *right panel*, the densities of the EGFR bands were quantified using ImageJ software and normalized against β-actin. Results from five individual experiments were plotted to show that EGFR degradation was enhanced in HDAC6 knock-down cells. *Error bar*, S.E. *, $p < 0.05$ in two tailed Student's *t* test. *B*, control and HDAC6 siRNA-transfected (3 days) cells were serum-starved and stimulated with EGF for indicated times. Cell lysates were prepared and analyzed by immunoblotting using anti-phosphotyrosine, anti-phospho-Erk 1/2, anti-Erk 1/2, anti-EGFR, and anti-HDAC6 antibodies.

cells were left at 37 °C for 15 min in pre-warmed DMEM to load the early endosomes with biotin-EGF. Next, the cells were washed, and cell surface-bound biotin-EGF was stripped using ice-cold 0.2 N acetate, 0.5 M NaCl (pH 4.5) for 1.5 min. After washing with cold DMEM, the cells were chased at 37 °C in DMEM containing 100 ng/ml unlabeled EGF for 15, 30, 60, and 90 min or for 90 min on ice as a control. When chase was completed, the culture medium was collected, and cells were washed with the stripping solution mentioned above. The materials stripped from the cell membranes were combined with the medium. The mixtures that contained recycled biotin-EGF were pH neutralized and captured on avidin-beads for 2 h at 4 °C. Extravidin-horseradish peroxidase was added to the beads and revealed by 1 mg/ml OPD and 0.015% H_2O_2. Cells chased on ice were lysed and biotin-EGF was determined as the total amount of internalized biotin-EGF. In addition, protein concentrations of the total cell lysates were determined using the Protein Assay kit (Bio-Rad) to normalize the amount of recycled biotin-EGF. A standard curve of optical density as a function of biotin-EGF was established using a serial dilution of biotin-EGF with known concentrations.

Immunoprecipitation and Immunoblotting—A549 cells were pretreated with 10 μg/ml cycloheximide for 30 min before cells were treated with 100 ng/ml EGF for times indicated in the figures. Cell lysates were prepared in 1% Triton X-100-PBS solution containing Protease Inhibitor Cocktail and Phosphatase Inhibitor Cocktail. Immunoprecipitation was carried out using monoclonal anti-EGFR antibody and protein G beads for 3 h at 4 °C. Samples were analyzed by immunoblotting following a standard protocol. The bands were revealed by ECL and recorded on x-ray film. To evaluate the degradation of EGFR, the intensity of EGFR bands from HDAC6 knock-down and control cells was scanned and quantified using ImageJ software.

Immunostaining for Flow Cytometry Assay—293T cells were co-transfected with pcDNA-EGFR and one of the α-tubulin constructs (GFP-α-tubulin WT, GFP-α-tubulin K40R, or GFP-α-tubulin K40Q) for 3 days. In the last 8 h of transfection, one group of cells received treatment of 1 μM TSA and 10 μg/ml cycloheximide. The control group was only treated with cycloheximide. After treatment, cells were detached by Accutase and fixed in 4% PFA for 2 h at room temperature or overnight at 4 °C. Permeabilization of the cell membrane was conducted in 0.2% Triton X-100. Anti-EGFR polyclonal antibody and goat anti-rabbit IgG Cy5 were used to label EGFR. Cells were examined by flow cytometry. Double transfected cells were gated, and total EGFR levels were evaluated from percentage of cells that were gated and the mean value of the fluorescence. EGFR in mutant tubulin-expressing and that in TSA-treated cells were compared with the total EGFR in non-TSA-treated GFP-α-tubulin WT-expressing cells.

RNA Analysis—For RNA analysis, HDAC6 in A549 cells were transiently knocked-down for 3 and 4 days. Cells were

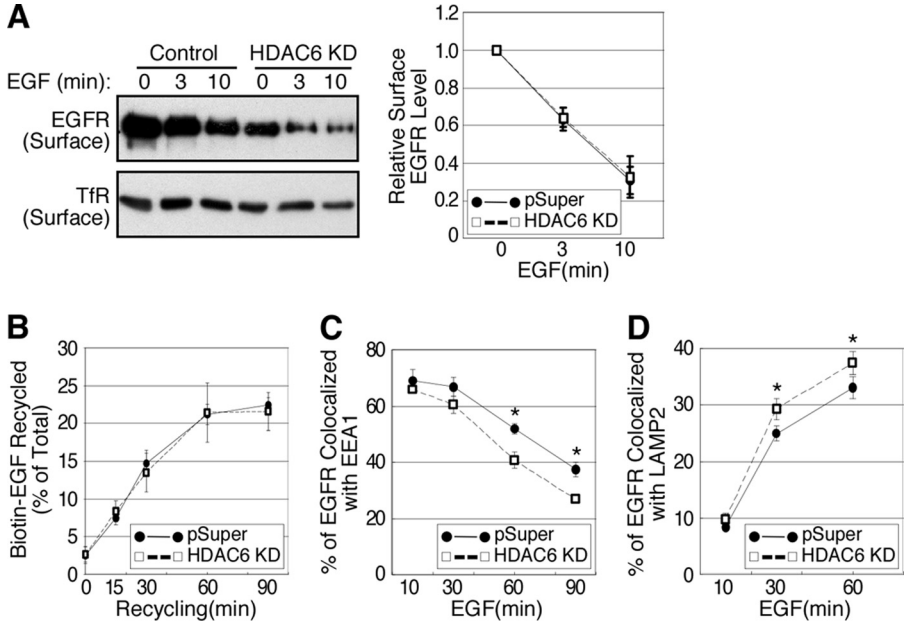

FIGURE 4. **HDAC6 regulates post-endocytic transport.** *A*, control and HDAC6 knock-down A549 cells were serum-starved overnight and were either left untreated or stimulated with 100 ng/ml EGF for 3 or 10 min. Cell surface proteins were biotin-labeled, pulled-down on avidin-beads, and analyzed by immunoblotting using anti-EGFR and anti-transferrin receptor antibodies (*left panel*). EGFR bands from four independent experiments were quantified and graphed (*right panel*). *Error bars*, S.E. *B*, A549 cells were serum-starved, processed to internalize biotin-EGF for 15 min, and chased for indicated times. Biotin-EGF reappeared in culture medium and on the cell surface, and was collected and quantified using a streptavidin-based colorimetric approach. Recycled biotin-EGF from five independent experiments was plotted. *Error bar*, S.E. *C*, A549 cells were serum-starved and stimulated with EGF for indicated periods of time. The cells were then processed for double labeling immunofluorescent microscopy using anti-EEA1 and anti-EGFR antibodies. Localization of EGFR to the EEA1-containing vesicles was analyzed using Image J software. *, $p < 0.05$ in two-tailed Student's *t* test, $n = 3$. *Error bar*, S.D. *D*, A549 cells were processed for double-labeling immunofluorescent microscopy as in *C*, except that anti-LAMP2 and anti-EGFR antibodies were used. Co-localization of EGFR to LAMP-2-containing vesicles was examined. *, $p < 0.05$ in two-tailed Student's *t* test, $n = 5$. *Error bar*, S.E.

washed quickly with PBS, and total RNA was prepared with Tri reagent (MRC) following the manufacturer's protocol. Total RNA was resuspended in DEPC water for RT-PCR analysis as described earlier (20). All real-time PCR values were normalized to 18 S rRNA.

RESULTS

HDAC6 Associates with the Endosomal Compartments—To investigate a possible regulatory role for HDAC6 in endocytic trafficking, we first examined whether HDAC6 associates with endocytosed EGFR. In human lung cancer A549 cells that received a short period of EGF treatment, HDAC6 showed mostly as puncta throughout the cells and HDAC6 colocalized with a portion but significant number of EGFR-containing early endosomes (labeled by EGF-Alexa Fluor 488 and early endosome marker EEA1, cycles in Fig. 1*A*), suggesting that HDAC6 interacts with the endosomal compartment. Because of the partial colocalization with the endosomes, HDAC6 might not be an integrative endosomal resident, but rather a factor in transient association with the endosomes. Similarly, at later time points, a portion of HDAC6 could be found in EGFR-positive vesicles that were also positive for CD63 (cycles in Fig. 1*B*), a marker for the late endosomes and lysosomes. To further verify the association of HDAC6 with late endosomes, we used the phosphoinositide 3-kinase inhibitor wortmannin to arrest endosomal progression at the stage of MVBs/late endosomes (21, 22). As shown in Fig. 1*C*, wortmannin treatment revealed prominent HDAC6 association with the EGFR-positive MVBs. Interestingly, similar to macropinosomes (12), some wortmannin-arrested endosomes were also positive for F-actin (Fig. 1*C*). By co-immunoprecipitation, we further examined the interaction of HDAC6 and the EGFR-loaded endosomes. We found that HDAC6 and EGFR were co-immunoprecipitated from the same protein complex. The interaction was significantly augmented after EGF treatment, concurrent with EGFR activation and post-internalization transport (Fig. 1*D*). Next, we took a different approach to analyze HDAC6 distribution by equilibrium density centrifugation in a discontinuous sucrose gradient. As shown in Fig. 1*E*, a small, but significant portion of HDAC6 was co-fractionated with EEA1 and EGFR (fractions 7–10). In addition, HDAC6 also peaked between fractions 11 and 13. The significance of this peak is still not clear at the present time. Altogether, these results indicate that a population of HDAC6 physically associates with the endosomal compartments.

HDAC6 Regulates EGFR Degradation—Based on the physical interaction of HDAC6 with the endosomes, we next investigated whether HDAC6 regulates EGFR endocytic trafficking and degradation. To this end, we first determined EGFR levels in A549 cells stably expressing a HDAC6-specific siRNA (15), or A549 cells that were transiently transfected with a different HDAC6-targeting siRNA. As shown in Fig. 2, *A* and *B*, EGFR protein was reduced in both HDAC6 knock-down situations, consistent with the finding in a recent report (23). Not only in A549 cells, a similar reduction of EGFR was also observed in human prostate cancer LNCaP cells and pancreatic cancer Panc-1 cells that were transiently treated with the HDAC6-specific siRNA (Fig. 2*C*). In comparison, Erk1 and Erk2, downstream targets of EGFR signaling, were not affected (Fig. 2*B*). The reduced levels of EGFR were not due to reduction of EGFR mRNA. On the contrary, EGFR messenger was increased in transient HDAC6 knock-down cells (Fig. 2*D*), probably a result of compensatory reaction to the lower amount of EGFR protein. Collectively, these data indicate that HDAC6 regulates EGFR level post-transcriptionally.

As ligand-induced degradation is the primary mechanism that controls EGFR levels, we next determined if HDAC6 affects EGFR degradation in response to EGF. As shown in Fig. 3, EGF-induced EGFR degradation was accelerated signifi-

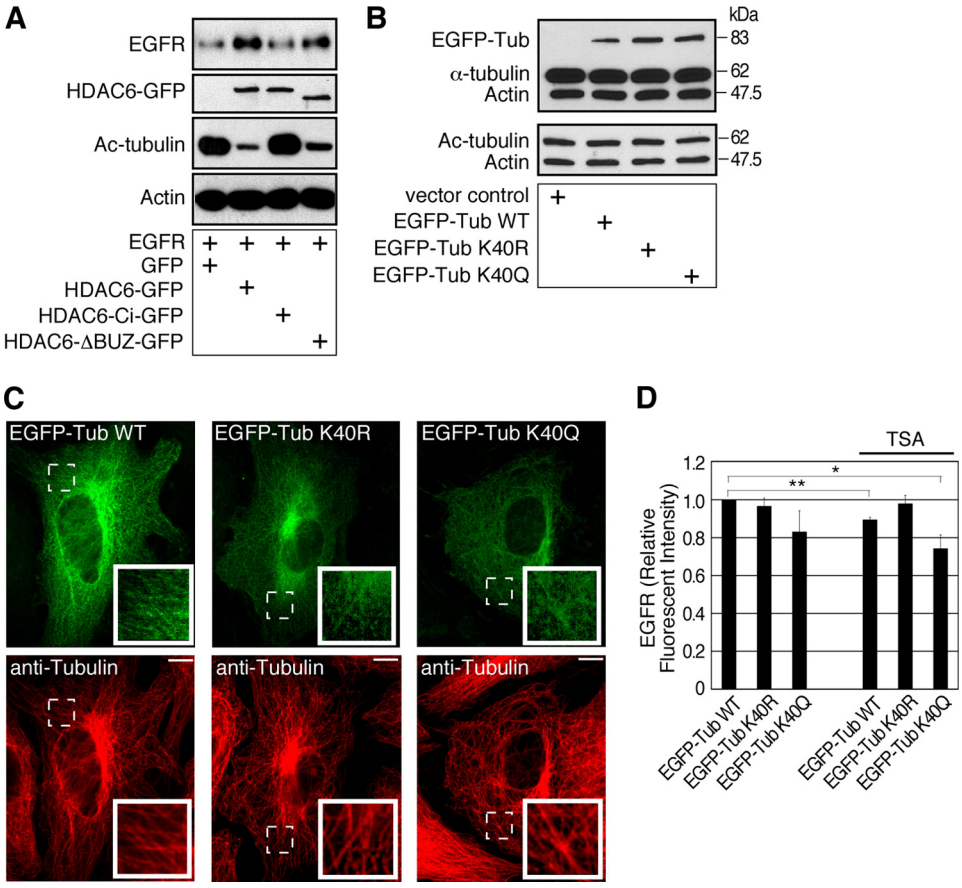

FIGURE 5. **Tubulin acetylation regulates EGFR in the cells.** *A*, HDAC6 knock-out MEFs re-expressing control GFP, HDAC6-GFP, HDAC6-Ci-GFP, or HDAC6-ΔBUZ-GFP were engineered to express EGFR. Cell lysates were examined by immunoblotting using anti-EGFR, anti-GFP, anti-acetyl-tubulin, and anti-β-actin antibodies. The EGFR level was inversely correlated to tubulin acetylation. (GFP band in GFP control group was not shown.) *B*, 293T cells were transfected for 3 days with a control vector, EGFP-α-tubulin WT, EGFP-α-tubulin K40R, or EGFP-α-tubulin K40Q plasmid. Cell lysates were examined by immunoblotting using a mixture of anti-α-tubulin and anti-β-actin antibodies, or a mixture of anti-acetylated tubulin and anti-β-actin antibodies. *C*, MEFs were transfected with constructs as in *B* for 2.5 days, and the microtubules were visualized by immunofluorescence using an anti-tubulin antibody. The exogenous EGFP-tagged α-tubulin became a part of the microtubule network. *Insets*, enlarged areas marked by *dotted lines*. *Bars*, 10 μm. *D*, 293T cells were co-transfected with EGFR-pcDNA and EGFP-α-tubulin WT, EGFP-α-tubulin K40R, or EGFP-α-tubulin K40Q for 3 days. For the last 8 h of transfection, cells were treated with only cycloheximide or TSA and cycloheximide. Cells were immunostained for EGFR and examined by flow cytometry. **, $p < 0.01$ and *, $p < 0.05$ in two-tailed and paired Student's *t* test, $n = 5$. *Error bars*, S.E.

cantly in HDAC6 knock-down cells (Fig. 3*A*). Consistently, EGFR activation and signaling were reduced in intensity and duration in HDAC6 knock-down cells (Fig. 3*B*).

HDAC6 Regulates EGFR Intracellular Transport—Aberrant EGFR stability could be the result of altered endocytosis and/or the subsequent intracellular trafficking of the receptors. To distinguish these possibilities, we first determined that the internalization of EGFR through analysis of the EGFR remained at the cell surface after EGF stimulation. As shown in Fig. 4*A*, the receptors were efficiently internalized in both cell types after EGF treatment, albeit HDAC6 knock-down cells had much reduced EGFR at the cell surface. Quantification of cytoplasmic membrane EGFR at different time points indicated that the kinetics of EGFR endocytosis were almost identical in both cell types, suggesting that HDAC6 does not significantly affect EGFR endocytosis. We next determined if HDAC6 regulates EGFR degradation by affecting its recycling. As shown in Fig. 4*B*, the kinetics of EGFR recycling were comparable in both control and HDAC6 knock-down cells. A maximum of about 22% of the internalized EGFR (indicated by biotin-EGF) were recycled to the plasma membrane in about an hour, similar to EGFR recycling described for A431 cells (19). Consistent with this observation, knock-down of HDAC6 also had little effect on cell surface transferrin receptor, which undergoes constitutive endocytosis and recycling to the cytoplasmic membrane (Fig. 4*A*, *bottom panel*). Taken together, our data indicate that HDAC6 does not have a prominent role in clathrin-dependent EGFR endocytosis or receptor recycling.

We then asked whether HDAC6 has a role in post-endocytic EGFR transport to late endosomes and lysosomes. While endocytosed EGFR moves away from early endosomes and progresses toward late endosomes, it segregates from the early endosomal marker EEA1. Consequently, the degree of co-localization of EGFR and EEA1 decreases with time. As shown in Fig. 4*C*, co-localization of EGFR and EEA1 was extensive and comparable in control and HDAC6 knock-down cells at the early time point after EGF treatment (10 min), consistent with our observation that HDAC6 did not appreciably affect EGFR endocytosis (Fig. 4*A*). However, at later time points, the number of vesicles that were positive for both EGFR and EEA1 decreased more quickly in HDAC6 knock-down cells than in control cells, suggesting that EGFR became segregated from the early endosomes faster in HDAC6-deficient cells (Fig. 4*C*). Supporting this conclusion, at later time points after EGF treatment, more EGFR was found to co-localize with the late endosome and lysosome marker LAMP2 in HDAC6 knock-down cells (Fig. 4*D*). Although the differences between the control and the HDAC6 knock-down cells in those co-localization assays are modest, it is possible that an accumulated effect from multiple rounds of enhanced EGFR trafficking could lead to prominent reduction of EGFR observed in HDAC6 knock-down cells (Fig. 2). Together, these findings strongly suggest that transport of the activated EGFR from the early endosomes to late endosomes/lysosomes is accelerated in HDAC6-deficient cells.

HDAC6 Deficiency Induces Microtubule Acetylation and Promotes Microtubule-mediated Endocytic Vesicle Transport—Cargo sorting from the early endosomes and subsequent cargo transport to the late endosomes are regulated by microtubules (2–6). As HDAC6 regulates tubulin acetylation, we considered

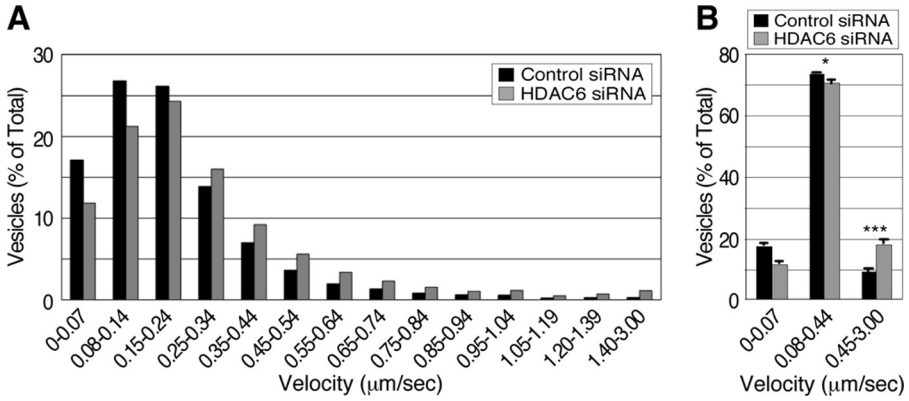

FIGURE 6. **HDAC6-dependent tubulin deacetylation regulates post-endocytic vesicle transport.** *A*, control and HDAC6 siRNA-treated (3 days) cells were serum-starved and treated with 80 ng/ml EGF-Alexa Fluor 488. The cells were then examined by video microscopy at a rate of 1 frame per second. Time-lapse image stacks were analyzed in MetaMorph, and the interval velocity of vesicle movement was recorded and pooled. The graph represents vesicle distribution against different velocity ranges. The high speed microtubule-dependent (0.45–3.00 μm/s) vesicle transport was enhanced in HDAC6 knock-down cells (*gray bars*) when compared to control cells (*closed bars*). *B*, vesicle mobility of control cells (*closed bars*) was compared with that of HDAC6 siRNA-treated cells (*gray bars*) in ranges of 0–0.07 μm/s, 0.08–0.44 μm/s (actin-dependent movement), and 0.45–3.00 μm/s. ***, $p < 0.0001$ and *, $p < 0.05$ in two-tailed Student's *t* test ($n = 12$).

the possibility that the enhanced EGFR degradation originated from HDAC6 deficiency involves the deregulation of microtubule-dependent endocytic vesicle trafficking. Specifically, hyperacetylation of tubulin results in higher affinity of motor proteins to microtubules (13, 14), which will lead to extended motor attachment and enhanced motor processivity on the cytoskeleton. To test this possibility, we first generated HDAC6-null mouse embryonic fibroblast lines that stably expressed GFP, wild-type HDAC6 (HDAC6-GFP), deacetylase-inactive HDAC6 (HDAC6-Ci-GFP), or binder of ubiquitin zinc finger (BUZ, (15)) domain-deleted HDAC6 (HDAC6-ΔBUZ-GFP) (12). These cells were then engineered to express human EGFR. As shown previously, the wild-type and the BUZ-deletion but not the deacetylase-inactive HDAC6 showed potent tubulin deacetylase activity (Fig. 5*A*) (12). Importantly, the EGFR levels increased significantly in wild-type HDAC6- and HDAC6-ΔBUZ-expressing cells. In stark contrast, EGFR level remained low in deacetylase-inactive HDAC6-expressing cells. Taken together, these observations suggest an inverse correlation between HDAC6-regulated tubulin acetylation and EGFR level.

To gain further evidence that the acetylation of tubulin affects EGFR levels, we assessed the effect of an acetylation-resistant tubulin mutant (lysine 40 → arginine; EGFP-α-tubulin K40R) and an acetylation-mimicking mutant (lysine 40 → glutamine; EGFP-α-tubulin K40Q). In transient transfection assays, wild-type tubulin, tubulin K40R, and K40Q mutants were expressed at a similar level, which was about 20% of the total α-tubulin in the cells (Fig. 5*B*). All constructs were able to incorporate into the microtubule network (Fig. 5*C*) (16). Under normal culture condition, EGFR levels were similar between EGFP-α-tubulin WT and EGFP-α-tubulin K40R-expressing cells, but EGFR was reduced in acetylation-mimicking EGFP-α-tubulin K40Q-expressing cells, in support of the proposition that acetylated microtubules accelerate EGFR degradation (Fig. 5*D*). Interestingly we also found that in control EGFP-α-tubulin WT-expressing cells, treatment with TSA, a pan-HDAC inhibitor that effectively inhibits HDAC6 activity, resulted in a modest but consistent reduction in EGFR level. However, TSA-induced reduction in EGFR was effectively reversed by the expression of acetylation-resistant EGFP-α-tubulin K40R mutant. In contrast, EGFR level was further reduced in acetylation-mimicking EGFP-α-tubulin K40Q expressing cells that were treated with TSA (Fig. 5*D*). Collectively, these results provide further support to the conclusion that tubulin acetylation negatively regulates EGFR levels.

Because tubulin acetylation affects microtubule affinity for motor proteins, we next determined whether HDAC6 regulates the transport of EGFR-bearing vesicles. To this end, endosomes in control and HDAC6 knock-down cells were labeled with EGF-Alexa Fluor 488 and their movements were evaluated by live cell imaging. Over 1,200 fluorescent EGF-labeled vesicles from 12 independent videos were randomly selected, and their movements were tracked and analyzed. We found that the population of vesicles with speed for microtubule-dependent transport (≥0.45 μm/s (13, 24)) were remarkably increased in HDAC6 knock-down cells by about 2-fold (Fig. 6, *A* and *B*). In contrast, vesicle mobility with interval velocity of 0.08–0.44 μm/s, representing F-actin-dependent transport (25, 26), was mildly reduced in HDAC6 knock-down cells. Together, these data suggest that acetylation of microtubules promotes the microtubule-directed transport of EGFR-loaded vesicles.

DISCUSSION

HDAC6 has been characterized as a microtubule-associated deacetylase. In this study, we presented new evidence that HDAC6 also associates with a subpopulation of endosomes (Fig. 1). This finding is of particular interest as we have previously shown that HDAC6 associates with macropinosomes, a form of clathrin-independent endocytic vesicles (12). Importantly, we found that loss of HDAC6 activity causes deregulation of the microtubule-dependent transport of EGFR-containing endosomal vesicles and subsequently EGFR degradation. These findings identify HDAC6 as a new regulatory factor in the intracellular trafficking network that controls EGFR stability.

HDAC6 is the dominant tubulin deacetylase whose inactivation leads to dramatic accumulation of acetylated microtubules (8, 12, 27). Although α-tubulin acetylation is one of the most common post-translational modifications of microtubules (7), its biological function has been elusive. In this study, we presented evidence that tubulin acetylation is functionally linked to endocytic trafficking. Elevation of microtubule acetylation resulting from the loss of HDAC6 activity enhances microtubule-directed transport of EGFR-containing endosomal vesi-

cles. Consequently, the transition of EGFR from early to late endosomes is accelerated, leading to augmented EGFR degradation. Recently, Reed *et al.* (14) showed that tubulin acetylation is required for efficient anterograde transport of JNK-interacting protein 1, a kinesin-1-associated cargo. Dompierre *et al.* (13) also examined the role of tubulin acetylation in the exocytosis of brain-derived neurotrophic factor (BDNF) and found that pharmacologically-induced hyperacetylation of tubulin is associated with increased flux of secretory vesicles and the secretion of BDNF. In light of these findings, our data would suggest that in cells deficient in HDAC6, either induced by HDAC6-specific siRNA or by TSA treatment, increased binding of dynein motor to the acetylated microtubules results in enhanced retrograde trafficking of EGFR-containing endosomes toward degradative endosomal compartments (Figs. 4 and 6). Because HDAC6 associates with both the dynein motor complexes (15) and the vesicles (this study), it is plausible that under normal conditions, recruitment of HDAC6 to specific endosomal vesicles would promote the deacetylation of microtubules locally, which in turn reduces motor processivity and vesicle movement. This regulation might be important to ensure an orderly and timely trafficking of EGFR-bearing vesicles. Deregulation of this process, as shown in HDAC6-deficient cells could lead to premature delivery of EGFR vesicles to the degradative compartment, resulting in accelerated receptor degradation and dampened downstream signaling (Fig. 3). Because HDAC6 does not affect EGFR endocytosis and recycling (Fig. 4*A*), our findings therefore highlight a specific role of HDAC6 in post-endocytic trafficking of EGFR, which could be important in determining the duration of EGFR signaling. Indeed, HDAC6 is required for efficient cancer cell growth and tumor development (28). The ability to modulate growth factor signaling through endocytic trafficking might underlie part of the pro-oncogenic activity of HDAC6. In conclusion, our study identifies HDAC6 as a novel component of the endocytic trafficking network, further implicating an important regulatory role for microtubule acetylation in vesicular trafficking and signaling.

Acknowledgments—We thank Drs. I. Dikic and M. C. Hung for exchanging data before publication. We thank Drs. C. Counter and B. Harvat for critically reading the manuscript.

REFERENCES

1. Yarden, Y. (2001) *Eur. J. Cancer* **37,** Suppl. 4, S3–S8
2. Aniento, F., Emans, N., Griffiths, G., and Gruenberg, J. (1993) *J. Cell Biol.* **123,** 1373–1387
3. Brown, C. L., Maier, K. C., Stauber, T., Ginkel, L. M., Wordeman, L., Vernos, I., and Schroer, T. A. (2005) *Traffic* **6,** 1114–1124
4. Loubéry, S., Wilhelm, C., Hurbain, I., Neveu, S., Louvard, D., and Coudrier, E. (2008) *Traffic* **9,** 492–509
5. Lakadamyali, M., Rust, M. J., Babcock, H. P., and Zhuang, X. (2003) *Proc. Natl. Acad. Sci. U.S.A.* **100,** 9280–9285
6. Driskell, O. J., Mironov, A., Allan, V. J., and Woodman, P. G. (2007) *Nat. Cell Biol.* **9,** 113–120
7. L'Hernault, S. W., and Rosenbaum, J. L. (1985) *Biochemistry* **24,** 473–478
8. Hubbert, C., Guardiola, A., Shao, R., Kawaguchi, Y., Ito, A., Nixon, A., Yoshida, M., Wang, X. F., and Yao, T. P. (2002) *Nature* **417,** 455–458
9. Kovacs, J. J., Murphy, P. J., Gaillard, S., Zhao, X., Wu, J. T., Nicchitta, C. V., Yoshida, M., Toft, D. O., Pratt, W. B., and Yao, T. P. (2005) *Mol. Cell* **18,** 601–607
10. Bali, P., Pranpat, M., Bradner, J., Balasis, M., Fiskus, W., Guo, F., Rocha, K., Kumaraswamy, S., Boyapalle, S., Atadja, P., Seto, E., and Bhalla, K. (2005) *J. Biol. Chem.* **280,** 26729–26734
11. Zhang, X., Yuan, Z., Zhang, Y., Yong, S., Salas-Burgos, A., Koomen, J., Olashaw, N., Parsons, J. T., Yang, X. J., Dent, S. R., Yao, T. P., Lane, W. S., and Seto, E. (2007) *Mol. Cell* **27,** 197–213
12. Gao, Y. S., Hubbert, C. C., Lu, J., Lee, Y. S., Lee, J. Y., and Yao, T. P. (2007) *Mol. Cell. Biol.* **27,** 8637–8647
13. Dompierre, J. P., Godin, J. D., Charrin, B. C., Cordelières, F. P., King, S. J., Humbert, S., and Saudou, F. (2007) *J. Neurosci.* **27,** 3571–3583
14. Reed, N. A., Cai, D., Blasius, T. L., Jih, G. T., Meyhofer, E., Gaertig, J., and Verhey, K. J. (2006) *Curr. Biol.* **16,** 2166–2172
15. Kawaguchi, Y., Kovacs, J. J., McLaurin, A., Vance, J. M., Ito, A., and Yao, T. P. (2003) *Cell* **115,** 727–738
16. Rusan, N. M., Fagerstrom, C. J., Yvon, A. M., and Wadsworth, P. (2001) *Mol. Biol. Cell* **12,** 971–980
17. Fu, L., Gao, Y. S., Tousson, A., Shah, A., Chen, T. L., Vertel, B. M., and Sztul, E. (2005) *Mol. Biol. Cell* **16,** 4905–4917
18. Gao, Y., and Sztul, E. (2001) *J. Cell Biol.* **152,** 877–894
19. Sorkin, A., Krolenko, S., Kudrjavtceva, N., Lazebnik, J., Teslenko, L., Soderquist, A. M., and Nikolsky, N. (1991) *J. Cell Biol.* **112,** 55–63
20. Cohen, T. J., Waddell, D. S., Barrientos, T., Lu, Z., Feng, G., Cox, G. A., Bodine, S. C., and Yao, T. P. (2007) *J. Biol. Chem.* **282,** 33752–33759
21. Fernandez-Borja, M., Wubbolts, R., Calafat, J., Janssen, H., Divecha, N., Dusseljee, S., and Neefjes, J. (1999) *Curr. Biol.* **9,** 55–58
22. Futter, C. E., Collinson, L. M., Backer, J. M., and Hopkins, C. R. (2001) *J. Cell Biol.* **155,** 1251–1264
23. Kamemura, K., Ito, A., Shimazu, T., Matsuyama, A., Maeda, S., Yao, T. P., Horinouchi, S., Khochbin, S., and Yoshida, M. (2008) *Biochem. Biophys. Res. Commun.* **374,** 84–89
24. Ha, J., Lo, K. W., Myers, K. R., Carr, T. M., Humsi, M. K., Rasoul, B. A., Segal, R. A., and Pfister, K. K. (2008) *J. Cell Biol.* **181,** 1027–1039
25. Merrifield, C. J., Moss, S. E., Ballestrem, C., Imhof, B. A., Giese, G., Wunderlich, I., and Almers, W. (1999) *Nat. Cell Biol.* **1,** 72–74
26. Taunton, J., Rowning, B. A., Coughlin, M. L., Wu, M., Moon, R. T., Mitchison, T. J., and Larabell, C. A. (2000) *J. Cell Biol.* **148,** 519–530
27. Matsuyama, A., Shimazu, T., Sumida, Y., Saito, A., Yoshimatsu, Y., Seigneurin-Berny, D., Osada, H., Komatsu, Y., Nishino, N., Khochbin, S., Horinouchi, S., and Yoshida, M. (2002) *EMBO J.* **21,** 6820–6831
28. Lee, Y. S., Lim, K. H., Guo, X., Kawaguchi, Y., Gao, Y., Barrientos, T., Ordentlich, P., Wang, X. F., Counter, C. M., and Yao, T. P. (2008) *Cancer Res.* **68,** 7561–7569